PERGAMON

Journal of Structural Geology 21 (1999) 251–257

JOURNAL OF STRUCTURAL GEOLOGY

# Mechanics of high displacement gradient faulting prior to lithification

Christopher A.J. Wibberley [a,*], Jean-Pierre Petit [a], Thierry Rives [b]

[a] *Laboratoire de Géophysique et Tectonique, Case 060, Université Montpellier 2, Place E. Bataillon, 34095 Montpellier Cédex 5, France*
[b] *Department Interpretation Structurale, Elf E&P, Avenue Larribau, 64018 Pau, France*

Received 17 August 1998; accepted 10 December 1998

**Abstract**

We present maximum displacement–length data from normal faults with strike half-lengths ranging from a few centimetres to 5 m. The data are from faults formed in sand prior to lithification in the Talaat n'Yacoub basin, High Atlas, Morocco. Our data typically have an order of magnitude higher average strike displacement gradients as compared to published data for normal faulting of lithified sedimentary rocks. Results are put in a context of strength and frictional parameters most likely to affect fault tip propagation using previous fault growth models. We show that an increase in shear modulus during lithification of sand into sandstone will outweigh the effect of increasing shear strength, resulting in longer faults for a given maximum displacement in lithified sedimentary rocks. 

## 1. Introduction

In an ideal model of displacement distribution on the surface of an isolated, blind fault, the displacement will be at a maximum in the centre ($d_{max}$), and decrease systematically towards the edges, which are defined as a single elliptical lines (Watterson, 1986; Walsh and Watterson, 1987, 1989). Recent work by Nicol et al. (1996) shows that fault tip lines often have a high chance of being restricted along part of their length by the development of other faults, thus modifying the tip line form. They agree, however, that the elliptical tip line model is a useful basic concept for isolated faults. The function by which this displacement variation occurs from centre to tip depends on the mechanism for fault growth and has been a topic of much discussion in the last decade (e.g. Walsh and Watterson, 1987; Marrett and Allmendinger, 1991; Cowie and Scholz, 1992; Gillespie et al., 1992; Dawers et al., 1993). The mechanical behaviour of the host rock, its response to the strain accrued by imposing a displacement variation along the fault, and response to fault tip stresses, is one of the most important considerations in fault mechanics, leading workers to interpret fault $d_{max}/L$ data in terms of mechanical properties of the faulted medium. Furthermore, it has been proposed that lithologies with lower shear moduli will have higher $d_{max}/L$ ratios than stiffer materials (e.g. Barnett et al., 1987; Walsh and Watterson, 1988; Gross et al., 1997), and graphical representation of this has been attempted (e.g. Walsh and Watterson, 1989). On the other hand, Cowie and Scholz (1992) proposed a model which suggests that material shear strength (in any given situation) is important in that stronger materials will have higher $d_{max}/L$ ratios, because of the increased ability of the material to support increased stresses at the fault tip. However, the Cowie and Scholz (1992) model also suggests that shear modulus should be important, with an increasing shear modulus decreasing the $d_{max}/L$ ratio as in the Walsh and Watterson (1988) case. Though not inherently related, shear modulus and shear strength often increase together, hence there may be competition between shear modulus and shear strength in controlling the length increase of a fault with displacement for different materials.

* Corresponding author. E-mail: wibbs@dstu.univ-montp2.fr

0191-8141/99 $ - see front matter 
PII: S0191-8141(99)00006-1

In this way, it has been recognised that lithology is an important control on fault array properties. However, whilst fruitful work on the role of lithological strength variations has been presented for different lithified rocks by Gross et al. (1997), the range in mechanical strengths of different lithologies examined in the literature is often not enough to demonstrate the role of the different material strength parameters on, say, the $d_{max}/L$ relationships of faults. Furthermore, data are often analysed over a wide range of scales on a log–log plot which tends to mask the variations. Further insights will only be gained by broadening the range of mechanical strengths examined, such as fault arrays in material deformed prior to its complete lithification. Previous studies of faults formed in sediments prior to complete lithification have demonstrated the potential importance of faulting throughout the history of sediment lithification, basin subsidence and deformation (Laville and Petit, 1984; Davison, 1987; Guiraud and Séguret, 1987; Higgs, 1988). Work here examines minor normal faults (over two orders of magnitude of scale) which affected quartzarenitic sands prior to their complete lithification. Data on displacement gradients are presented and compared with published data from coarse-grained sedimentary rocks over a range of scales. The contrasting $d_{max}/L$ ratios of these pre-lithification faults against the published data are discussed in terms of the contrasting material properties and their likely controls on fault propagation.

## 2. Data on faulting prior to lithification

### 2.1. Regional setting

Outcrops of Triassic sandstone were examined from exhumed Triassic basins associated with the Tizi n'Test fault zone in the High Atlas, Morocco, which contains evidence of both NNW–SSE extension and left-lateral ENE–WSW strike-slip faulting during sedimentation (Petit and Beauchamp, 1986). Despite basin inversion during the Alpine-related thrusting of the High Atlas mountains, the Triassic structures in these basins are preserved, where sandstones display small- to large-scale evidence of faulting prior to complete lithification (Petit and Laville, 1987). We present observations from the Idni area (Fig. 1) where bedding planes of sandstone units show well-exposed faults. The faults we examined have maximum displacements from 3 to 100 mm. These fault arrays appear similar to those in lithified rocks, often in the conjugate arrangement, with strike patterns revealing fault tips in isolated segments (e.g. Walsh and Watterson, 1988), relay ramps (e.g. Peacock and Sanderson, 1991), branching and many other features similar to outcrop and larger scale fault arrays in lithified rock. However, under close examination in the field (confirmed by microstructural work), these faults do not exhibit grain-size reduction or slickenside surfaces whitened by quartz grain crushing which characterises Alpine-related faults here (Petit and Laville, 1987). Exposed surfaces occasionally show rough lineations indicating the slip direction, the scale of the ridges and grooves defining these lineations being generally one order of magnitude larger than the grain size. In other words, these faults are typical disaggregation zones described by many authors from modern faulted sediments (e.g. Knipe, 1986a) prior to lithification of the material. A burial depth of between 200 and 500 m at the time of faulting was estimated from mapping data on the overlying upper Triassic siltstone series and stratigraphic column construction (Petit and Laville, 1987).

### 2.2. Fault displacement gradient measurements

Small-displacement normal faults were studied from bedding plane exposures, and along-strike displace-

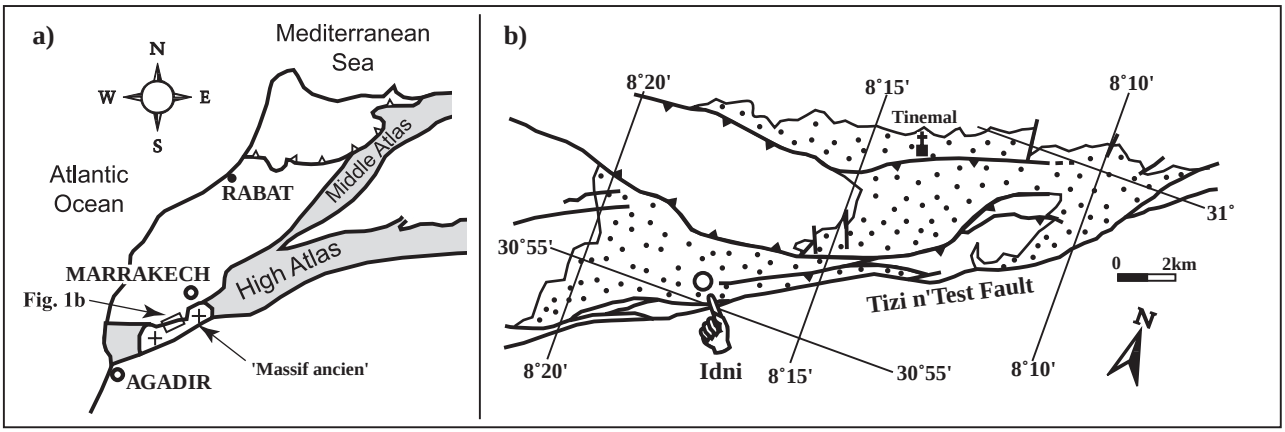


Fig. 1. Geographical and structural setting of the study area. (a) Morocco and the High Atlas Mountains. (b) The Talaat n'Yacoub Basin (stippled) and the location of the study area. All bold lines represent map-scale faults, those with barbs being inverted normal faults.

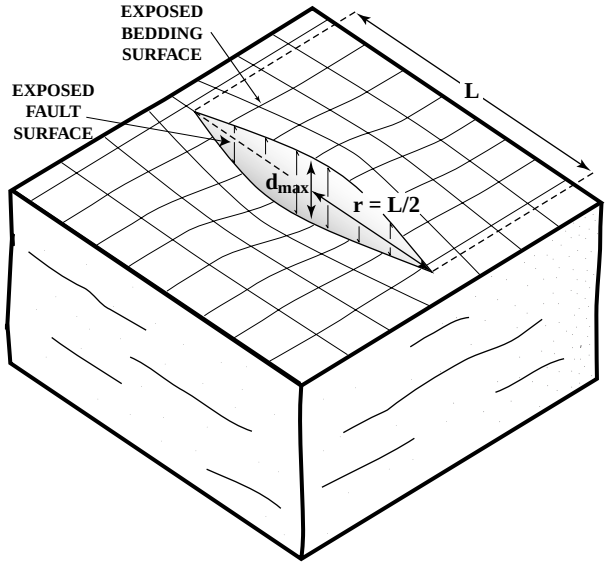


Fig. 2. Cartoon depicting fault dimension parameters. The cross-hatch pattern depicts the upper side of a bedding surface.

ment gradients (normal to the displacement direction) were assessed (Fig. 2). Only simple isolated fault segments were used, where a maximum displacement gradient decreases to a single fault tip, with no branching or relay ramping to transfer the displacement to another fault, or confuse an assessment of centre-to-tip displacement variations in any other way (Gross et al., 1997). For each fault an average value of displacement gradient is inferred by only considering the displacement maximum, and not at other points along the fault traces. Although high local variations in displacement gradient have been documented along some normal faults (e.g. Cartwright and Mansfield, 1998), these were not observed to be significant in most of the examples in this study. We follow the procedure of Peacock and Sanderson (1991) in considering the data in terms of $r$ (distance between fault tip and point of maximum displacement on the fault profile) and $d_{max}$ (maximum displacement on the fault profile), but present values of $0.5d_{max}/r$, to give an easily interpretable value of displacement gradient in each wall from a central line (Fig. 2). This measure gives a direct reflection of the wall rock shear strain and also is equivalent to $d_{max}/L$ values for 'ideal' fault ellipses (which will be symmetric), and can make use of displacement gradient data for faults where only one end is isolated. Because $r$ was measured parallel to the outcrop surface (bedding plane), this value will only give a true measure of fault half length if the fault slip vector is exactly dip–slip when the bedding is back-rotated to the horizontal. Deviations from this ideal case may induce small errors but consideration of elliptical geometry shows that, for example, a deviation of the slip vector by 10° from this ideal dip-slip pitch will result in an error of 5% in fault length measurement, whereas our analysis is more concerned with orders of magnitude variation, so this error will not be significant. Fault profiles which do not intersect the centre of the fault ellipse (chords) will not display a true value either of $d_{max}$, or of $L$, but some lower values than an 'ideal' profile. Furthermore, the relationship between $d_{max}$ and $L$ is likely to change. Muraoka and Kamata (1983) showed in their fig. 11 how such 'off-centre' fault profiles will have lower $d_{max}/L$ values for their choice of displacement distribution on an ideal fault surface (as will be the case for most 'reasonable' displacement distributions). As we do not know a priori the position of a fault profile with respect to the true fault centre, many of the data here are probably minimum estimates of the true fault $d_{max}/L$ values. This may explain much of the scatter in $d_{max}/L$ data of isolated fault data sets. However, the fact that this source of error will exist for most data sets from outcrop-scale fault profiles means that it is nevertheless valid to compare our Idni data with previously published data sets, especially when we are concerned with order-of-magnitude differences between data sets.

At the Idni locality, outcrops were studied from where such measurements could be made. In this case, three orientation groups were found:

Set 1: NW–SE-striking, subvertical normal faults, downthrown to the NE.

Set 2: NE–SW-striking, very steeply dipping towards the east, with oblique sinistral kinematics.

Set 3: N–S-striking, downthrown and dipping moderately (20–60°) to the west.

Back-tilting of bedding to horizontal shows that sets 1 and 3 are conjugate normal fault types, with original 60° dips towards the NE and SW, respectively. Set 2 is a later set of cross faults which offsets the earlier faults. Most of the faults in set 2 show the same textures of faulting prior to lithification as sets 1 and 3, but a major throughgoing fault of set 2 also has mineralisation and growth fibre lineations possibly due to post lithification reactivation, and is not used in our data set.

### 2.3. Comparison with published data sets

Fig. 3(a) presents data on measured $0.5d_{max}$ vs $r$ for these three sets of faults, on a linear scale. Data sets of the same scale range from interbedded sandstones and siltstones (Muraoka and Kamata, 1983), limestones (Peacock and Sanderson, 1991) and high porosity sandstones (Fossen and Hesthammer, 1997) are also plotted for comparison. It should be noted here, that from the Peacock and Sanderson (1991) data set, only those data are used where simple displacement gradients to fault tips occurred without branching or relay

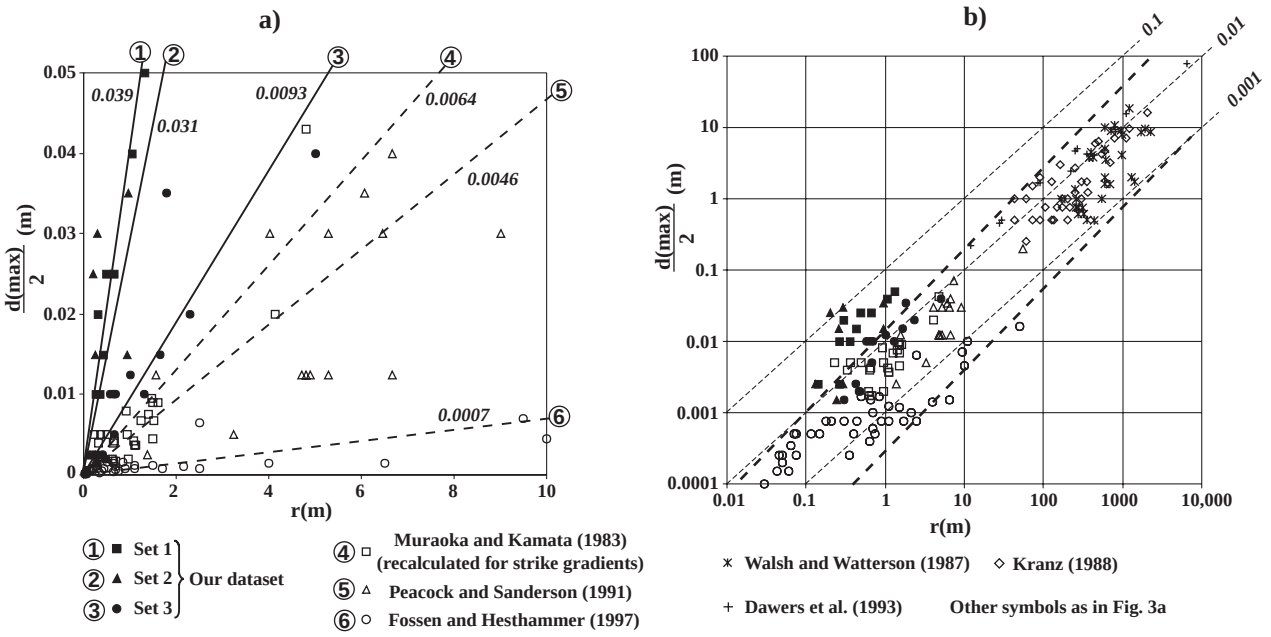


Fig. 3. (a) Graph of $d_{max}/2$ vs $r$ for the fault profiles examined at Idni, and other published data sets of comparable scale. Bold lines are best fit linear trends for each Idni data set, whilst dashed lines are for other data sets, with numbers in italics showing calculated gradients of best fit lines. (b) The same data on a logarithmic graph, also including other published data sets over a wider scale range. Thin dashed lines are displacement gradient contours, with values labelled. Bold dashed lines are general bounds to all these published data, with computed gradients of 1.1.

ramping to affect the systematic displacement variations towards an isolated fault tip. Normally only data measuring displacement gradients normal to the displacement direction should be considered comparable. However we include the data of Muraoka and Kamata (1983), who measured down-dip displacement variations on normal faults, because few published data sets exist at the same scale as ours. Nicol et al. (1996) calculated an average strike-dimension to dip-dimension ratio of 2.15 for blind isolated normal faults in their data sets, hence the data of Muraoka and Kamata (1983) are tentatively replotted with our data after the $r$ values were multiplied by 2.15 (Fig. 3a). From the statement in the Muraoka and Kamata (1983) article that their data samples 'faults developed in Quaternary lacustrine sediments', many authors have assumed that these data reflect faulting in unlithified material, and possibly incorrectly interpreted the data using this assumption. In fact, the nature of the fault zones and fault rocks is more akin to brittle faulting of lithified material (Muraoka, personal communication, 1997), so we treat their data as representative of faulting in lithified rock. Such confusion may have arisen over the usage of the term 'sediments' in more than one sense (see Maltman, 1984).

Fig. 3(a) shows that the faults at Idni generally have much higher displacement gradients than faults from the Muraoka and Kamata (1983), Peacock and Sanderson (1991) and Fossen and Hesthammer (1997) data sets. The best fit lines on Fig. 3(a) are forced to go through the origin. They are a general guide only to the values of displacement gradients for each data set. Clearly, there is a lot of scatter, even after we have eliminated the effects of displacement transfer onto other faults and segment linkage by being careful in the data we used. Displacement gradients determined from $0.5d_{max}/r$ (Fig. 3a) range from 0.012 to 0.250 (average 0.078) for the Idni fault set 1 and from 0.0192 to 0.138 (average 0.062) for Idni fault set 2. These are an order of magnitude higher than those from isolated half-faults in limestone (from Peacock and Sanderson, 1991), and from one to two orders of magnitude higher than the deformation bands in high porosity sandstone (from Fossen and Hesthammer, 1997). Furthermore, all data sets from Idni have on average significantly higher displacement gradients than the data set of Muraoka and Kamata (1983) in sandstones and siltsones (Fig. 3a). In Fig. 3(b) the published data sets used were selected to be as representative as possible of displacement gradients from isolated normal faults or half-faults in coarse-grained lithified rocks without the effects of fault truncation, branching, fault linkage or relay ramping (hence rendering many published data sets inappropriate for comparison here). The higher $0.5d_{max}$ to $r$ ratios of our data are illustrated in Fig. 3(b) by their position higher and to the left of the published data from faulting of lithified material with the conclusion that our data set from faults affecting material prior to its lithification have larger $0.5d_{max}/r$ than published data on faulting of lithified rock.

## 3. Discussion

### 3.1. Implications for fault growth

In this section we relate our observations to the role of mechanical parameters on fault propagation. Clearly, shear modulus and shear strength may be important, yet their interplay in controlling idealised single fault propagation has not in the past been made clear. Cowie and Scholz (1992) presented a theoretical plot of shear strength ($\sigma_0$) vs $d_{max}/L$ for various values of shear modulus and used published data sets of $d_{max}/L$ and estimated shear moduli to make inferences on likely shear strengths. In order to do this, the residual frictional strength ($\sigma_f$) on the fault (i.e. the shear resistance to frictional sliding at any one point on the fault, which, like shear strength, is depth dependent) also needs to be taken into account. Here, to interpret the interplay between the material shear properties and their influences on $d_{max}/L$ ratios, we consider the Cowie and Scholz (1992) model in terms of $(\sigma_0 - \sigma_f)$ vs shear modulus ($\mu$) to give a more readily interpretable graph. Rewriting the Cowie and Scholz (1992) eq. (10) in terms of $(\sigma_0 - \sigma_f)$ we obtain:

$$(\sigma_0 - \sigma_f) = \frac{\mu \cdot (d_{max}/L)}{A} \quad (1)$$

where $A$ is considered a constant in our analysis, being related to Poisson's ratio ($\nu$) and the inelastic tip zone length to total fault length ratio ($s/L$), given that $\theta_2 = \cos^{-1}(1 - 2(s/L))$ (Cowie and Scholz, 1992), by the equation

$$A = \frac{(1-\nu)}{2\pi} \cdot \left[\cos\theta_2 \cdot \log_e \frac{(\sin\theta_2 + 1)^2}{(\sin\theta_2 - 1)^2}\right]. \quad (2)$$

Consideration of $A$ as a constant is justified because trial plots of $(\sigma_0 - \sigma_f)$ vs $\mu$ for various reasonable values of $\nu$ and $s/L$ showed that the plot is very insensitive to these parameters. Values of $\nu = 0.2$ and $s/L = 0.18$ were used (as by Cowie and Scholz, 1992) in Eq. (2) to obtain $A = 0.332$, enabling Eq. (1) to be plotted as a simple linear function, for various values of $d_{max}/L$. Using the $d_{max}/L$ data presented in Fig. 3 and generalised values of shear modulus of sand and of sandstone, areas on the graph of Fig. 4 are plotted to represent the cases of un- or partially lithified sand, and of lithified sandstone, acknowledging that these areas may be quite wide because many factors can contribute to the material properties considered, such as composition, grain size, grain angularity, and water content in the sediment. The arrow between the two fields illustrates the difference in shear modulus and $(\sigma_0 - \sigma_f)$ for the un- or partially lithified case and the lithified case. We tentitatively write 'lithification' along this arrow, although it is recognised that the pathway

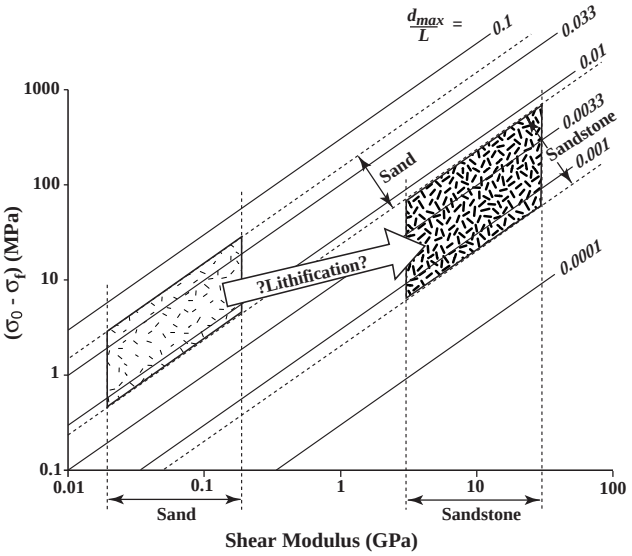


Fig. 4. Graph of $(\sigma_0 - \sigma_f)$ vs shear modulus, with contour lines of displacement gradient, drawn from Eq. (1) using $A = 0.332$ (see text). On the graph are marked areas representing approximate values for unlithified sand (lightly stippled area), and for lithified sandstone (densely stippled area). These areas are drawn corresponding to the $d_{max}/L$ data presented in Fig. 3 using the Idni data sets for the unlithified sand, and the other data sets for the lithified case. Shear modulus values are derived from a number of standard geological engineering and soil mechanics sources.

from sediment to sedimentary rock will depend on many factors affecting these parameters during compaction and diagenesis which are beyond the scope of this study. More complicated scenarios are probable when one considers the processes operating during continuous lithification in a geologically real situation during deformation. For example, the change in deformation mechanisms with increasing confining stress from particulate flow to cataclastic grain size reduction has been demonstrated (Lucus and Moore, 1986). Furthermore, during lithification, many processes involved in the progressive stages of diagenesis (e.g. Knipe, 1986b) and compaction can each have effects on material behaviour (see for example Maltman, 1994; and in particular, Byrne, 1994) and consequent fault zone structure (Ishimaru and Miyata, 1991). Finally, application of the critical state concept to deforming sediments which are being affected by both burial and tectonic stresses demonstrates a variation in deformation response and the onset of failure for sediments at different stages of compaction and stress state (e.g. Jones and Addis, 1986).

### 3.2. Effect of fault zone plasticity

Fig. 4 shows how $(\sigma_0 - \sigma_f)$ values in the order of 1–10 MPa are derived from Eq. (1) for the case of faulting in un- or partially lithified sand. The term $(\sigma_0 - \sigma_f)$ is, according to the Coulomb criterion, cohesion.

However, cohesion in unlithified sand is much smaller than the range of $(\sigma_0 - \sigma_f)$ values suggested in Fig. 4, and is often taken to be zero. Instead we can regard $(\sigma_0 - \sigma_f)$ as a softening term, expressing the difference in shear strengths of the intact material and fault zone. This softening effect is often written:

$$(\sigma_0 - \sigma_f) = \Delta C_{material} + \Delta\sigma_{rh} \quad (3)$$

where $\Delta C_{material}$ is material softening (reduction of cohesion and angle of internal friction by cataclastic deformation of the fault zone material), and $\Delta\sigma_{rh}$ is 'non-associated plasticity softening' (Vermeer, 1990) due to the decrease of mean stress inside the plastically deforming fault zone where the principal stress axes rotate so that stress and strain are coaxial. Vermeer (1990) considered this with elastic unloading allowed outside the fault zone so that the state of stress inside the fault zone is different from that outside, and this approach has recently been favourably contrasted against simpler elastic and rigid-plastic theories in the prediction of fault array geometries (Gerbault et al., 1998). Vermeer (1990) showed how the peak shear stress ($\tau$) to normal stress ($\sigma_n$) ratio at plastic fault zone formation reduces to a residual shear stress to normal stress ratio during fault zone shear. This can be viewed as being due to plastic slip zones (e.g. Riedel shears) within the fault zone being non-parallel to the fault, so that a Mohr circle analysis gives a lower shear stress for continued slip than was required for initial failure (e.g. Lockner and Byerlee, 1993), assuming that normal stress on the fault zone remains constant. For an angle of friction $\phi$, $(\tau/\sigma_n)_{peak} = \tan\phi$ and, for a non-dilating sand, $(\tau/\sigma_n)_{residual} = \sin\phi$ (Vermeer, 1990). This allows us to write (Poliakov, personal communication, 1998):

$$(\sigma_0 - \sigma_f) = \sigma_n(\tan\phi - \sin\phi) + \Delta C_{material}. \quad (4)$$

For the case of unlithified sand we assume cohesion and material softening to be negligible and focus on the role of non-associated plasticity softening. By assuming the approximation $\sigma_n = \rho g h$ (where $\rho$ = average sediment density $\sim$2200 kg m$^{-3}$, $g$ = acceleration due to gravity $\sim$10 m s$^{-2}$ and $h$ is the burial depth at the time of deformation) a range of $(\sigma_0 - \sigma_f)$ can be estimated for $\phi$ from 30 to 45° and $h$ from 200 to 500 m. For these values, Eq. (4) gives $(\sigma_0 - \sigma_f)$ of 0.46–4.4 MPa which falls within the range of values predicted for the un- or partially lithified sediment field in Fig. 4, at least for the lower shear modulus values. Hence a mechanism of non-associated plasticity softening on these faults is consistent with the $(\sigma_0 - \sigma_f)$ values for the un- or partially lithified sediment predicted by the Cowie and Scholz (1992) fault growth model.

## 4. Conclusions

Data presented in this paper show that faults affecting un- or partially lithified sand can have higher displacement to length ratios than those affecting lithified rock. Analysis of factors affecting fault tip propagation, using the Cowie and Scholz (1992) fault growth model, suggest that the lower shear modulus for unlithified sand (where compared against a sandstone) will be a more important factor than the lower stress drop. Calculated stress drop values much higher than sand cohesion can be attributed to non-associated plasticity softening of the faults. Finally, these findings may provide a further criterion for the recognition of 'soft-sediment' faults, especially useful for structural geologists working in the petroleum industry where identifying faults formed prior to lithification in core for example can constrain the timing of deformation.

## Acknowledgements

Research was supported by an Elf Aquitaine research grant to the first author. Field assistance from P. Cortes and M. Amarhar, and the kindness of the people from Idni was greatly appreciated during the course of the fieldwork. Discussions with Alexei Poliakov on the physics of faulting, Paul Jouanna from an engineering perspective and Hirofumi Muraoka on the data helped clarify aspects of interpretation. Comments on an earlier draft by John Fletcher and an anonymous reviewer, and reviews by Hakkon Fossen and Jim Evans helped improve the manuscript.

## References

Barnett, J.A.M., Mortimer, J., Rippon, J.H., Walsh, J.J., Watterson, J., 1987. Displacement geometry in the volume containing a single normal fault. American Association of Petroleum Geologists Bulletin 71, 925–937.

Byrne, T., 1994. Sediment deformation, dewatering and diagenesis: illustrations from selected mélange zones. In: Maltman, A.J. (Ed.), The Geological Deformation of Sediments. Chapman & Hall, London, pp. 239–259.

Cartwright, J.A., Mansfield, C.S., 1998. Lateral displacement variation and lateral tip geometry of normal faults in the Canyonlands National Park, Utah. Journal of Structural Geology 20, 3–19.

Cowie, P.A., Scholz, C.H., 1992. Physical explanation for the displacement–length relationship of faults using a post-yield fracture mechanics model. Journal of Structural Geology 14, 1133–1148.

Davison, I., 1987. Normal fault geometry related to sediment compaction and burial. Journal of Structural Geology 9, 393–401.

Dawers, N.H., Anders, M.H., Scholz, C.H., 1993. Growth of normal faults: Displacement–length scaling. Geology 21, 1107–1110.

Fossen, H., Hesthammer, J., 1997. Geometric analysis and scaling relations of deformation bands in porous sandstone. Journal of Structural Geology 19, 1479–1493.

Gerbault, M., Poliakov, A.N.B., Daignieres, M., 1998. Prediction of faulting from the theories of elasticity and plasticity: what are the limits? Journal of Structural Geology 20, 301–320.

Gillespie, P.A., Walsh, J.J., Watterson, J., 1992. Limitations of dimension and displacement data from single faults and the consequences for data analysis and interpretation. Journal of Structural Geology 14, 1157–1172.

Gross, M.R., Gutiérrez-Alonso, G., Bai, T., Wacker, M.A., Collinsworth, K.B., Behl, R., 1997. Influence of mechanical stratigraphy and kinematics on fault scaling relationships. Journal of Structural Geology 19, 171–183.

Guiraud, M., Séguret, M., 1987. Soft-sediment microfaulting related to compaction within the fluvio-deltaic infill of the Soria strike-slip basin (northern Spain). In: Jones, M.E., Preston, R.M.F. (Eds.), Deformation of Sediments and Sedimentary Rocks. Geological Society Special Publication 29, pp. 123–136.

Higgs, B., 1988. Syn-sedimentary structural controls on basin deformation in the Gulf of Corinth, Greece. Basin Research 1, 155–165.

Ishimaru, K., Miyata, Y., 1991. Morphology of shear planes in soft-sediments—effects of compaction load and sediment composition. Journal of the Geological Society of Japan 97, 713–727.

Jones, M.E., Addis, M.A., 1986. The application of stress path and critical state analysis to sediment deformation. Journal of Structural Geology 8, 575–580.

Knipe, R.J., 1986a. Faulting mechanisms in slope sediments: Examples from deep sea drilling project cores. In: Moore, J.C. (Ed.), Structural Fabrics in Deep Sea Drilling Project Cores from Forearcs. Geological Society of America Memoir 166, pp. 45–54.

Knipe, R.J., 1986b. Deformation mechanism path diagrams for sediments undergoing lithification. In: Moore, J.C. (Ed.), Structural Fabrics in Deep Sea Drilling Project Cores from Forearcs. Geological Society of America Memoir 166, pp. 151–160.

Krantz, R.W., 1988. Multiple fault sets and three-dimensional strain: theory and application. Journal of Structural Geology 10, 225–237.

Laville, E., Petit, J.-P., 1984. Role of synsedimentary strike-slip faults in the formation of Moroccan Triassic basins. Geology 12, 424–427.

Lockner, D.A., Byerlee, J.D., 1993. How geometric constraints contribute to the weakness of mature faults. Nature 363, 250–252.

Lucus, S.E., Moore, J.C., 1986. Cataclastic deformation in accretionary wedges: Deep Sea Drilling Project Leg 66, southern Mexico, and on-land examples from Barbados and Kodiak Islands. In: Moore, J.C. (Ed.), Structural Fabrics in Deep Sea Drilling Project Cores from Forearcs. Geological Society of America Memoir 166, pp. 89–103.

Maltman, A.J., 1984. On the term 'soft sediment deformation'. Journal of Structural Geology 6, 589–592.

Maltman, A.J. (Ed.), 1994. The Geological Deformation of Sediments. Chapman & Hall, London.

Marrett, R., Allmendinger, R.W., 1991. Estimates of strain due to brittle faulting: sampling of fault populations. Journal of Structural Geology 13, 735–738.

Muraoka, H., Kamata, H., 1983. Displacement distribution along minor fault traces. Journal of Structural Geology 5, 483–495.

Nicol, A., Watterson, J., Walsh, J.J., Childs, C., 1996. The shapes, major axis orientations and displacement patterns of fault surfaces. Journal of Structural Geology 18, 235–248.

Peacock, D.C.P., Sanderson, D.J., 1991. Displacements, segment linkage and relay ramps in normal fault zones. Journal of Structural Geology 13, 721–733.

Petit, J.-P., Beauchamp, J., 1986. Synsedimentary faulting and paleocurrent patterns in the Triassic sandstones of the High Atlas (Morocco). Sedimentology 33, 817–829.

Petit, J.-P., Laville, E., 1987. Morphology and microstructures of hydroplastic slickensides in sandstone. In: Jones, M.E., Preston, R.M.F. (Eds.), Deformation of Sediments and Sedimentary Rocks. Geological Society Special Publication 29, pp. 107–121.

Vermeer, P.A., 1990. The orientation of shear bands in biaxial tests. Géotechnique 40, 223–236.

Walsh, J.J., Watterson, J., 1987. Distribution of cumulative displacement and seismic slip on a single normal fault surface. Journal of Structural Geology 9, 1039–1046.

Walsh, J.J., Watterson, J., 1988. Analysis of the relationship between displacements and dimensions of faults. Journal of Structural Geology 10, 239–247.

Walsh, J.J., Watterson, J., 1989. Displacement gradients on fault surfaces. Journal of Structural Geology 11, 307–316.

Watterson, J., 1986. Fault dimensions, displacements and growth. Pure and Applied Geophysics 124, 365–372.